


Article

Estimation of Actual Evapotranspiration Using Satellite-Based Surface Energy Balance Derived from Landsat Imagery in Northern Thailand

Teerawat Suwanlertcharoen ¹, Thodsapol Chaturabul ², Thanaporn Supriyasilp ^{3,*}  and Kobkiat Pongput ¹

¹ Department of Water Resources Engineering, Faculty of Engineering, Kasetsart University, Bangkhen Campus, Bangkok 10900, Thailand

² Department of Civil and Environmental Engineering, Faculty of Science and Engineering, Kasetsart University, Chalermphrakiat Sakon Nakhon Province Campus, Sakon Nakhon 47000, Thailand

³ Department of Civil Engineering, Faculty of Engineering, Chiang Mai University, Chiang Mai 50200, Thailand

* Correspondence: thanaporn@eng.cmu.ac.th; Tel.: +66-53-94-4157

Abstract: In this study, satellite-based measures of surface energy balance and the mapping evapotranspiration at high resolution with internalized calibration (METRIC) from Landsat imagery were used to estimate the spatiotemporal distribution of actual evapotranspiration (ET_a) in northern Thailand, constituting a procedure that has rarely been performed in southeast Asia. Subsequently, we compared the ET_a obtained from METRIC with that calculated using the FAO-56 dual-crop coefficient method via the SIMDualKc software and found a strong correlation. An assessment of the accuracy of all the sample plots revealed the R^2 , Root-Mean-Square Error (RMSE), and mean absolute error (MAE) values to be 0.830, 0.730, and 0.575 mm d⁻¹, respectively. Differences in the cumulative ET_a values derived from SIMDualKc and METRIC ranged in magnitude from 0.93–3.57% for rice and 3.08–7.99% for longan. The ET_a values for forestland and waterbodies were higher than those for agricultural areas and areas with other forms of land use. The spatiotemporal distribution of the seasonal ET_a during the dry season was consistent with the climate, vegetation, and anthropogenic activity. Thus, our results indicate that METRIC is a reliable tool for estimating ET_a for water resource management under different environmental conditions and improving water use efficiency over large areas.

Keywords: METRIC; evapotranspiration; surface energy balance; Landsat; water balance



Citation: Suwanlertcharoen, T.; Chaturabul, T.; Supriyasilp, T.; Pongput, K. Estimation of Actual Evapotranspiration Using Satellite-Based Surface Energy Balance Derived from Landsat Imagery in Northern Thailand. *Water* **2023**, *15*, 450. <https://doi.org/10.3390/w15030450>

Academic Editors: Mladen Todorovic, Nada Mzid, Vito Cantore, Rossella Albrizio and Guido D'Urso

Received: 19 December 2022

Revised: 10 January 2023

Accepted: 18 January 2023

Published: 22 January 2023



Copyright: © 2023 by the authors. Licensee MDPI, Basel, Switzerland. This article is an open access article distributed under the terms and conditions of the Creative Commons Attribution (CC BY) license (<https://creativecommons.org/licenses/by/4.0/>).

1. Introduction

Southeast Asia is one of the world's most vital agricultural regions, accounting for 15% of food production in Asia and 7.7% globally [1]. Thailand, located in the southeastern region of the continent of Asia, covers an area of 513,120 km², with 43% of the country devoted to agricultural land [2]. Thailand is the foremost longan-producing country globally and produced approximately 0.98 million metric tons of longan from 2015–2017 [3].

At present, many parts of the world are affected by water scarcity, including Thailand. Higher food demands and population growth have directly affected water use in the agricultural and other sectors. Additionally, climate change has increased water scarcity and drought, with potential impacts including increased evapotranspiration and decreased water availability [4]. Consequently, the demand for water in agriculture and for irrigation water use have increased.

Longan orchards occupy a considerable portion of the agricultural land area in northern Thailand. Longan trees are susceptible to drought during the flowering and early fruit development stages, which generally occur during the dry season from the end of October to mid-May [5]. Premium fruit can only be produced under intensive water and nutrient management. In addition to longan, rice is commonly cultivated in this area, and also

requires a large amount of water during the dry season, especially in flooded paddies. The Upper Ping River Basin, which is one of the headwaters of the Chao Phraya River Basin, is located in northern Thailand. To understand crop water consumption over large areas and achieve effective water resource management, it is necessary to estimate the spatiotemporal distribution of actual evapotranspiration (ET_a) in agricultural areas, especially in longan orchards and paddy fields.

Evapotranspiration (ET) is an important component of water balance associated with the hydrological cycle and biological processes [6] and represents the total water loss from the Earth's surface, including water evaporated from the soil surface and that has transpired through plants. Therefore, the accurate estimation of the actual ET (ET_a) rate is crucial for understanding changes in water availability and sustainably managing water resources.

According to Allen et al. [7], ET data can be obtained using various measurement techniques, such as lysimeters, the Bowen ratio, the eddy covariance, sap flow, root zone soil water balance, and even satellite-based remote sensing, as well as direct modelling. Among these techniques, direct measurement techniques necessitate extensive experimental care and are susceptible to biases based on reported results [7]. Satellite imagery-based techniques can be used to estimate ET using the energy balance and can potentially be applied over large areas to identify regions characterised by ET reductions due to water stress [7]. The surface energy balance algorithm for land (SEBAL) [8] and mapping evapotranspiration at high resolution with internalized calibration (METRIC) [9] models are two widely used satellite-based surface energy balance techniques in which thermal infrared sensors are utilised to estimate ET_a . The METRIC model, which is a variant of the image-processing tool SEBAL, is used to estimate ET_a from the energy balance residual at the Earth's surface. Moreover, METRIC has been enhanced to provide better integration with ground weather station data used to compute reference ET and has been applied to satellite images obtained using thermal infrared sensors such as the moderate resolution imaging spectroradiometer (MODIS) and Landsat [10]. Remote-sensing-based energy balance models have major limitations, such as time gaps, because remote-sensing images can only be obtained at a specific location on a periodic basis. Therefore, the effects of evaporation caused by precipitation events that occur between these time gaps may be overlooked [7]. Another technique that uses remote-sensing image data involves satellite-based vegetation indices (VIs). In this method, VIs obtained from image data are used to estimate the crop coefficient (K_c) and 'basal' crop coefficient (K_{cb}) by determining the relationship between the VI and these coefficients. A typical VI is the normalised difference vegetation index (NDVI). The 'basal' K_{cb} condition is a condition under which the soil surface is dry enough to reduce evaporation from the soil surface to relatively low levels compared with transpiration. However, transpiration continues to occur [7]. A reliable soil water balance model would be able to estimate soil water behaviour over time, thereby helping to overcome the majority of the difficulties in estimating ET from observations of soil water via direct modelling [7]. The advantages and disadvantages of these ET measurement techniques have previously been discussed by Allen et al. [7].

In Thailand, several approaches have been used to estimate ET with satellite-based remote sensing at spatial resolutions from regional to global scales. Zheng et al. [11] estimated ET with satellite-based Earth observation datasets as the primary inputs to derive daily ET in north-eastern Thailand. Sriwongsitanon et al. [12] validated ET values from seven global remote-sensing products used for water resource management in Thailand. Furthermore, other researchers have applied satellite-based surface energy balance using the SEBAL model to estimate ET_a from MODIS and Landsat-7 images in the Chao Phraya River Basin [13] and from Landsat-5 images in the Lam Ta Kong Basin [14]. However, to date, no studies using high-resolution satellite-based images and employing the METRIC model, which can provide better integration with data from ground weather stations than SEBAL for ET_a estimation at the field scale, have been conducted in Thailand. Therefore, it is of interest to study the accuracy of ET_a estimation using METRIC and Landsat-8 images in this region.

To our knowledge, few researchers have studied the accuracy of satellite-based ET_a values obtained using the soil water balance method. However, Paço et al. [15] analysed and compared the ET and crop coefficients of olive orchards obtained using the SIMDualKc and METRIC algorithms. They reported that the ET_a values obtained from the SIMDualKc and METRIC algorithms were similar, and that the crop coefficients derived from each model showed comparable patterns throughout the year. Thus, although the SIMDualKc and METRIC algorithms represent different approaches, their results appear to be comparable and complementary with respect to spatiotemporal scale. Furthermore, Tasumi [16] compared the ET_a value obtained from METRIC to that estimated independently using the FAO-56 single-crop approach. However, ET_a estimation based on surface energy balance using the METRIC model with a 30 m spatial resolution has rarely been performed in Southeast Asia, and the dual-crop coefficient method and SIMDualKc model have seldom been utilised for the evaluation of ET_a , especially in Thailand.

Herein, we focus on the estimation of ET over a large area for water management purposes using two approaches. First, we combine the METRIC algorithm and NDVI to overcome the time gap limitation and use Landsat images, which currently represent the highest resolution (a spatial resolution of 30 m) over a large area with a revisit time of 16 d. Thermal Landsat imagery can be used to evaluate vegetation phenology in the growing period and observe changes in the water stress of plants [17]. In the second approach, we apply direct soil water balance modelling using SIMDualKc. The SIMDualKc model employs the FAO-56 dual-crop coefficient method to estimate the crop ET. Then, we compare the results obtained with the two approaches.

The objectives of this study are as follows: (1) to estimate ET_a during each crop growth period using the METRIC model and Landsat-8 satellite data; (2) to evaluate the ET_a obtained from the METRIC model relative to the ET_a calculated from the FAO-56 dual-crop coefficient method; and (3) to study the spatiotemporal distribution of the ET_a for various land-use types in order to enhance water resource management in northern Thailand.

The ET_a obtained from the satellite-based surface energy balance data derived from Landsat imagery can be applied in water management schemes based on appropriate technology at field to regional scales, thereby covering a large area. These data are beneficial with respect to monitoring crop water use and stress. Furthermore, ET_a estimates based on the METRIC model can be used for water resource management planning and the localisation of water to meet irrigation water requirements in the dry season, especially in cultivation areas on both sides of the Ping River in the Chiang Mai and Lamphun provinces. The accurate estimation of the spatiotemporal distribution of ET_a in the Upper Ping Basin will allow for the establishment of better irrigation strategies, enhanced water use efficiency, and increased crop production yields.

2. Materials and Methods

2.1. Study Area

The research area was divided into two sections: the study area, which was the entire area used to study the spatiotemporal distribution of the ET_a across various land-use types, and the testing area, which was used to compare the ET_a obtained from the METRIC model and the FAO-56 dual-crop coefficient method (Figure 1).

The study area (~12,900 km² located in the plains of the upper northern region of Thailand along the Ping River (Figure 1b)), includes a variety of land utilisation areas, especially agricultural zones in irrigated areas, such as government, private, and community irrigation systems, and non-irrigated agricultural areas in the Chiang Mai and Lamphun provinces. Most of the agricultural portions consist of longan orchards and paddy fields. The general climate of this area is affected by southwest and northeast monsoons, and the annual climate is influenced by depression from the South China Sea between July and September, causing heavy rain from May to October. The mean annual temperature is 26.1 °C. The highest and lowest temperatures are 30 °C (in April) and 21.3 °C (in December), respectively. The average annual precipitation is 993.2 mm [18]. Types of land

use in the study area include forestland, orchards, urban and built-up land, paddy fields, miscellaneous land, field crops, perennial trees, waterbodies, and horticulture, accounting for 65.88%, 10.20%, 7.02%, 6.95%, 4.49%, 2.61%, 1.10%, 1.08%, and 0.67% of the entire area, respectively.

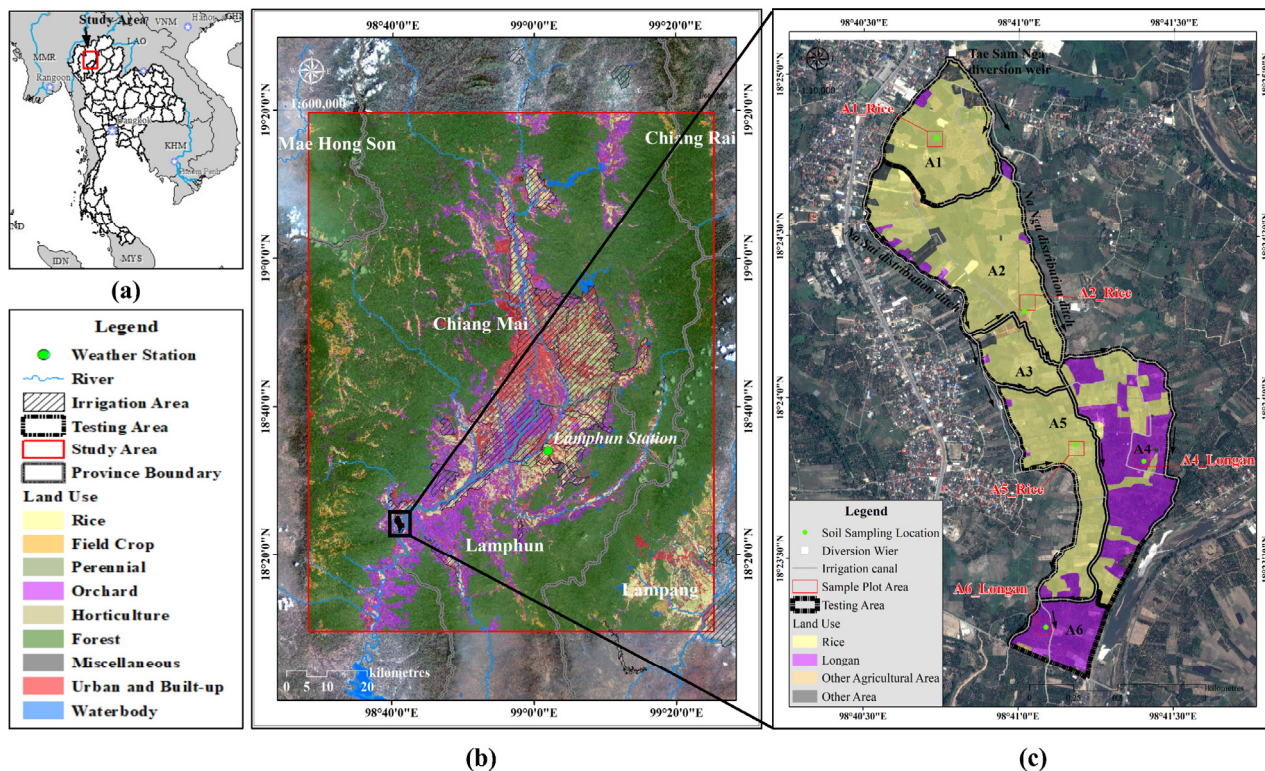


Figure 1. Study and testing areas: (a) general location of the study area in Thailand; (b) location of the study areas in the Chiang Mai and Lamphun provinces, which are situated in the plains of the upper northern region of Thailand along the Ping River; (c) testing area, which forms part of the Muang Luang Irrigation Project located in the Chom Thong District, Chiang Mai Province, downstream of the Muang Luang Weir.

To evaluate the ET_a obtained from the METRIC model, the FAO-56 dual-crop coefficient method was used. The testing area used for ET_a evaluation is part of the Muang Luang Irrigation Project located in the Chom Thong District, Chiang Mai Province (Figure 1c). The Muang Luang Weir is located upstream of this area. Paddy fields and longan orchards cover ~ 68% and 26% of the total area, respectively, and the Tae Sam Nga diversion weir, which splits into three irrigation canals, occupies the northern boundary. The testing area covers 2.12 km² and is located between the Na Sai and Na Ngu ditches [19].

2.2. Data

2.2.1. Satellite Imagery

In this study, Landsat-8 Operational Land Imager (OLI) and Thermal Infrared Sensor (TIRS) images with a 30 m spatial resolution were collected from level-1 products with terrain precision correction (L1TP) using U.S. Geological Survey (USGS) Earth Explorer. In total, 41 Landsat-8 OLI/TIRS images (Path 131/Row 47) were collected under cloud-free conditions throughout the crop growth period in the dry season from October 2017 to May 2020 as shown in Table 1 (12, 14, and 15 images for 2018, 2019, and 2020, respectively).

Table 1. Landsat-8 OLI/TIRS images (Path 131/Row 47) for the study area.

Dry Season in Year 2018			Dry Season in Year 2019			Dry Season in Year 2020		
Date	Day of Year (DOY)	Time of Acquisition (hh:mm:ss) [UTC+7]	Date	Day of Year (DOY)	Time of Acquisition (hh:mm:ss) [UTC+7]	Date	Day of Year (DOY)	Time of Acquisition (hh:mm:ss) [UTC+7]
22 Oct 2017	295	10:49:14	9 Oct 2018	282	10:48:44	12 Oct 2019	285	10:49:19
9 Dec 2017	343	10:49:04	25 Oct 2018	298	10:48:49	28 Oct 2019	301	10:49:19
25 Dec 2017	359	10:49:07	26 Nov 2018	330	10:48:51	13 Nov 2019	317	10:49:17
10 Jan 2018	10	10:49:01	28 Dec 2018	362	10:48:48	29 Nov 2019	333	10:49:15
26 Jan 2018	26	10:48:52	13 Jan 2019	13	10:48:46	15 Dec 2019	349	10:49:13
11 Feb 2018	42	10:48:45	29 Jan 2019	29	10:48:42	31 Dec 2019	365	10:49:09
27 Feb 2018	58	10:48:39	14 Feb 2019	45	10:48:40	16 Jan 2020	16	10:49:06
15 Mar 2018	74	10:48:30	2 Mar 2019	61	10:48:36	1 Feb 2020	32	10:49:01
31 Mar 2018	90	10:48:23	18 Mar 2019	77	10:48:31	17 Feb 2020	48	10:48:57
16 Apr 2018	106	10:48:14	3 Apr 2019	93	10:48:28	4 Mar 2020	64	10:48:52
18 May 2018	138	10:47:54	19 Apr 2019	109	10:48:22	20 Mar 2020	80	10:48:45
3 Jun 2018	154	10:47:43	5 May 2019	125	10:48:23	5 Apr 2020	96	10:48:35
			21 May 2019	141	10:48:33	21 Apr 2020	112	10:48:29
			6 Jun 2019	157	10:48:42	7 May 2020	128	10:48:20
						23 May 2020	144	10:48:22

2.2.2. Meteorological Data

Meteorological data for this study were obtained from the closest weather station in order to compute the standardised alfalfa reference ET equation (ET_r) and provide the inputs required for METRIC computations. The weather station records meteorological data every 10 min, including precipitation, air temperature, wind speed, relative humidity, and atmospheric pressure. Data were collected at the Lamphun station using the Automatic Weather System (AWS) of the Thailand Meteorological Department. The only climate data not available at this station were solar radiation data. Therefore, solar radiation data were derived from the air temperature difference using the Hargreaves–Samani radiation formula, which is an option available for calculating solar radiation on the REF-ET software. These meteorological data, except for precipitation, were also used to compute the daily standardised grass reference ET (ET_o) for the Muang Luang testing area. Precipitation data for this area were collected at Chom Thong station. The ET_o and precipitation data were then used as inputs for SIMDualKc. Precipitation data were obtained from different stations. For the study area (red square in Figure 1a), precipitation data from Lamphun station were chosen for METRIC computations. For the testing area, precipitation data from Chom Thong station were used.

2.2.3. Geographic Information System (GIS) Data

The GIS data required for this study consisted of land-use, irrigated area, and digital elevation model (DEM) data. Land-use data were obtained from the Land Development Department, whereas data regarding the irrigated area were obtained from the Royal Irrigation Department. For the DEM, Shuttle Radar Topography Mission (SRTM) data with 30 m spatial resolution were used, which were obtained from the USGS Earth Resources Observation and Science (EROS) Centre. The DEM was then used to calculate the slope and aspect of the area. The slope and aspect were later combined with the latitude, declination, hour angle, and solar incidence to obtain solar angles, which were then utilised to calculate the incoming shortwave radiation ($R_{S\downarrow}$) and net radiation (R_n), respectively.

2.2.4. Soil Sampling

Soil samples were taken from five plots to obtain soil texture information. The main soil type in most plots (A2_Rice, A5_Rice, and A6_Longan) was sandy loam, while the soil types of the A1_Rice and A4_Longan plots were loam and sandy clay loam, respectively.

These soil properties were necessary for the soil water balance calculation and estimation of ET_a using the FAO-56 dual-crop coefficient method. The sampling locations and soil properties are summarised in Table 2.

Table 2. Summary of soil properties for each plot in testing area.

Plot Name	Soil Texture	Sand (%)	Silt (%)	Clay (%)	Rock (%)	Location
A1_Rice	Loam	49.3	33.7	17	7.87	18°24'48.1" N, 98°40'44.1" E
A2_Rice	Sandy Loam	64	19	17	18.24	18°24'16.2" N, 98°41'01.1" E
A4_Longan	Sandy Clay Loam	45.8	25	29.2	15.4	18°23'48.2" N, 98°41'24.3" E
A5_Rice	Sandy Loam	64	22.8	13.2	0.14	18°23'51.4" N, 98°41'11.0" E
A6_Longan	Sandy Loam	67.9	20.6	11.5	0.77	18°23'17.4" N, 98°41'05.4" E

2.2.5. Water Use and Water Measurement in the Testing Area

According to the data obtained by Supriyasilp and Pongput [20], water from various sources is used in the dry season in the testing area, including rainfall, irrigation water supplied from the upstream Muang Luang Irrigation Scheme, irrigation water supplied from two pumping stations on the Ping River, and ponds. The proportions of the total amounts of water derived from each source are 11%, 15%, 57%, 16%, and 1%, respectively. The flow data observed in the dry season were measured from 21 March to 15 May 2019. The agricultural water supply for this testing area is jointly managed by the water management committee and farmers.

Descriptions and sources of the datasets used in this study are summarised in Table 3.

Table 3. Datasets used in this study.

Dataset	Description	Source
Satellite imagery	Landsat-8 Operational Land Imager (OLI) and Thermal Infrared Sensor (TIRS) images with 30 m spatial resolution were collected from level-1 products with terrain precision correction (L1TP)	USGS Earth Explorer (https://earthexplorer.usgs.gov/) (accessed on 3 January 2013)
Meteorological data	The Automatic Weather System (AWS) from the Lamphun station records meteorological data every 10 min, including the precipitation, air temperature, wind speed, relative humidity, and atmospheric pressure. In addition, precipitation data were collected at the Chom Thong station.	Thailand Meteorological Department
Digital Elevation Model (DEM)	Shuttle Radar Topography Mission (SRTM) data with 30 m spatial resolution	USGS Earth Resources Observation and Science (EROS) Centre
Land Use	GIS data regarding land-use classification at 1:25,000 scale	Land Development Department, Thailand
Irrigated Area	GIS data of irrigated area at 1:50,000 scale	Royal Irrigation Department, Thailand
Soil Sampling	Soil properties for each plot in testing area	Soil samples were taken from sample plots in testing area
Water Use and Water Measurement	Water supplied from various sources and the flow data observed in the dry season were measured from 21 March to 15 May 2019 in testing area	According to Supriyasilp and Pongput [20]

2.3. Software

Four software products were used in this study. Their capabilities are presented in Table 4.

Table 4. Software used in this study.

Software	Capabilities
ArcGIS 10.3.1	Image processing, spatial analysis, spatial statistics, mapping, visualisation, and exploration for estimation of satellite-based ET_a .
SIMDualKc	Estimation of ET_a using the FAO-56 dual-crop coefficient method.
REF-ET	Calculation of the reference ET.
DATimeS	Fill data gaps and generate the time series of daily ET_{rF} and NDVI image using the cubic spline interpolation method.

2.4. Overview of Methods

An outline of the methods, procedures, and subsequent workflow used in this study is presented in Figure 2.

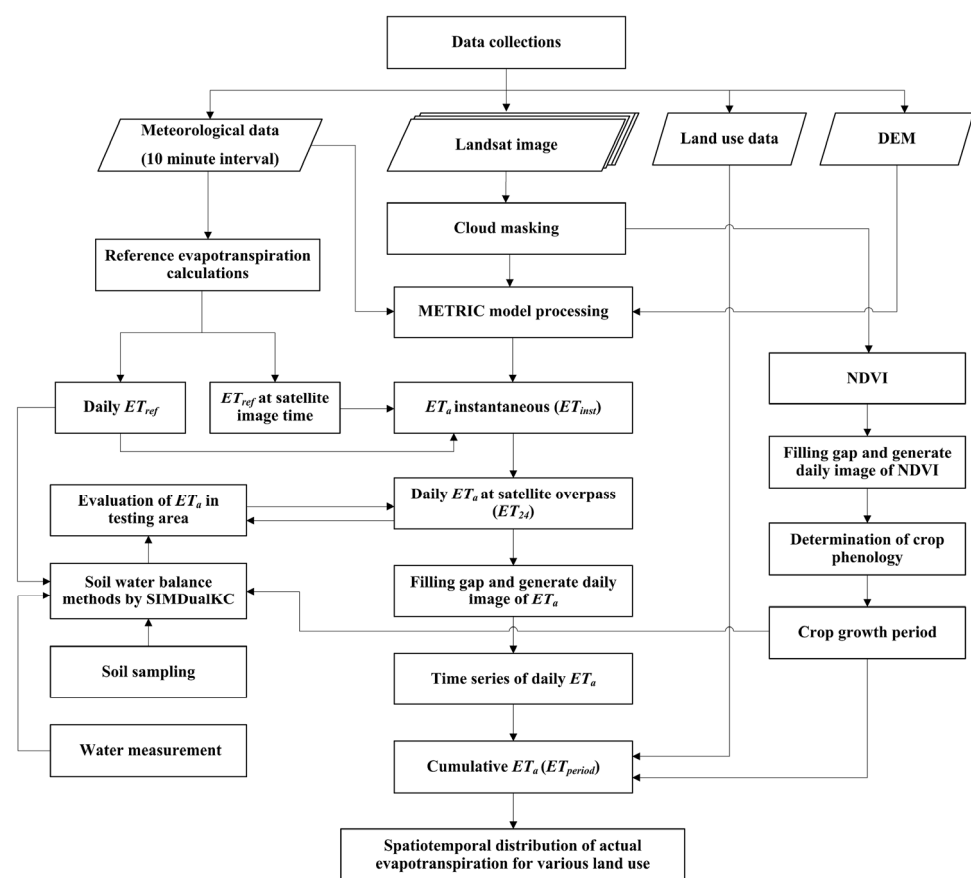


Figure 2. Frameworks and workflow for estimating actual evapotranspiration (ET_a) during each crop growth period using the METRIC model and Landsat-8 satellite data; evaluating the ET_a obtained from the METRIC model relative to the ET_a calculated using the FAO-56 dual-crop coefficient method; and studying the spatiotemporal distribution of the ET_a for various land-use types to improve water resource management in northern Thailand.

2.4.1. METRIC Model

The METRIC model was used to estimate the ET_a from remote-sensing data including satellite images at the time of image acquisition. The resulting ET_a value is called instantaneous ET. As part of the surface energy balance method, energy consumed by the ET process was calculated as the residual from the surface energy balance equation [9]:

$$LE = R_n - G - H, \tag{1}$$

where LE is the latent heat flux consumed by ET ($\text{W}\cdot\text{m}^{-2}$), R_n is the net radiation ($\text{W}\cdot\text{m}^{-2}$), G is the soil heat flux conducted into the ground ($\text{W}\cdot\text{m}^{-2}$), and H is the sensible heat flux transferred to the atmosphere ($\text{W}\cdot\text{m}^{-2}$).

The parameter R_n was calculated from the surface reflectance and temperature at the time of satellite image acquisition by summing incoming and outgoing shortwave and longwave radiation, including solar and thermal radiation [9]:

$$R_n = R_{S\downarrow} - \alpha R_{S\downarrow} + R_{L\downarrow} - R_{L\uparrow} - (1 - \varepsilon_o)R_{L\downarrow} \quad (2)$$

where R_n is the net radiation ($\text{W}\cdot\text{m}^{-2}$), $R_{S\downarrow}$ is the incoming shortwave radiation ($\text{W}\cdot\text{m}^{-2}$), α is the surface albedo (dimensionless), $R_{L\downarrow}$ is the incoming longwave radiation ($\text{W}\cdot\text{m}^{-2}$), $R_{L\uparrow}$ is the outgoing longwave radiation ($\text{W}\cdot\text{m}^{-2}$), and ε_o is the surface thermal emissivity (dimensionless).

Soil heat flux (G) is the magnitude of the soil energy stored or convected into the ground and can be computed as follows [21]:

$$\frac{G}{R_n} = 0.05 + 0.18e^{-0.521LAI}, \quad (3)$$

$$LAI \geq 0.5;$$

$$\frac{G}{R_n} = \frac{180 (T_s - 273.16)}{R_n + 0.084}, \quad (4)$$

$$LAI < 0.5,$$

where LAI is the leaf area index (dimensionless) and T_s is the land surface temperature (Kelvin).

Sensible heat flux transferred to the atmosphere (H) was calculated from the aerodynamic function-based heat transfer. The METRIC model was estimated based on a calibration using inverse modelling under extreme conditions (CIMEC) [22]. This method involves the selection of pixels with near-extreme conditions (hot and cold anchor pixels) on whose basis ET_a can be estimated and assigned. The sensible heat flux was calculated as follows:

$$H = \rho_{air} C_p \frac{dT}{r_{ah}} \quad (5)$$

where ρ_{air} is the air density ($\text{kg}\cdot\text{m}^{-3}$), C_p is the specific heat of air under constant pressure ($1004 \cdot \text{J}\cdot\text{kg}^{-1}\cdot\text{K}^{-1}$), dT is the near-surface temperature difference between the two near-surface heights z_1 (0.1 m) and z_2 (2 m; Kelvin), and r_{ah} is the aerodynamic resistance to heat transport ($\text{s}\cdot\text{m}^{-1}$).

Note that dT was solved using linear regression between dT and T_s of hot and cold anchor pixels selected from different areas under two extreme conditions. Cold and hot conditions were selected for the full vegetation canopy area and empty agricultural fields without vegetation cover, respectively.

Based on the calculation of the LE process as the residual from the surface energy balance equation, LE was calculated as the ET_a during the time of satellite image acquisition:

$$ET_{inst} = 3600 \times \frac{LE}{\lambda \rho_w}, \quad (6)$$

where ET_{inst} is the instantaneous ET_a at the moment of satellite image acquisition ($\text{mm}\cdot\text{h}^{-1}$), 3600 is the factor for the conversion from seconds to hours, ρ_w is the density of water ($100 \text{ kg}\cdot\text{m}^{-3}$), and λ is the latent heat of vaporisation ($\text{J}\cdot\text{kg}^{-1}$), which is calculated as $\lambda = [2.51 - 0.00236 (T_s - 273.15)] \times 10^6$.

In this step, the daily ET_a (ET_{24}) of each pixel was calculated as follows:

$$ET_{24} = \frac{ET_{inst}}{ET_r} * ET_{r24}, \quad (7)$$

where ET_{inst} is the instantaneous ET_a at the time of the satellite image acquisition ($\text{mm}\cdot\text{h}^{-1}$); ET_r is the alfalfa reference ET at the moment of satellite image acquisition, which is calculated at the weather station ($\text{mm}\cdot\text{h}^{-1}$); ET_{r24} is the daily alfalfa reference ET ($\text{mm}\cdot\text{day}^{-1}$); and ET_{24} is the daily ET_a ($\text{mm}\cdot\text{day}^{-1}$).

The ET_{inst}/ET_r ratio is the reference ET fraction (ET_rF) and is the same as the well-known K_c [9].

The ET_rF at the date of the image acquisition was interpolated with the cubic spline interpolation method to obtain the time series of the daily ET_rF . Subsequently, the daily ET_a (ET_{24}) was calculated by multiplying the daily ET_rF by ET_r .

The cumulative ET_a can be calculated for any period, such as a month or season, using the time series of the daily ET_a (ET_{24}) and the following equation:

$$ET_{period} = \sum_{i=m}^n ET_rF_i \times ET_{r24i}, \quad (8)$$

where ET_{period} is the cumulative ET_a for the period starting on day m and ending on day n , ET_rF_i is the reference evapotranspiration fraction for day i , and ET_{r24i} is the daily ET_a for day i .

2.4.2. Reference Evapotranspiration Calculation

The standardised Penman–Monteith equation for ET_{ref} has been proposed by the American Society of Civil Engineers (ASCE) for both the grass reference (ET_o) and alfalfa reference (ET_r) according to the format adopted in FAO-56 [6,17]

$$ET_{ref} = \frac{0.408\Delta(R_n - G) + \gamma \frac{C_n}{(T+273)} u_2 (e_s - e_a)}{\Delta + \gamma(1 + C_d u_2)}, \quad (9)$$

where ET_{ref} is the reference ET ($\text{mm}\cdot\text{day}^{-1}$ or $\text{mm}\cdot\text{h}^{-1}$), R_n is the net radiation ($\text{MJ m}^{-2} \text{d}^{-1}$ or $\text{MJ m}^{-2} \text{h}^{-1}$), G is the soil heat flux transferred to the ground ($\text{MJ m}^{-2} \text{d}^{-1}$ or $\text{MJ m}^{-2} \text{h}^{-1}$), T is the mean daily or hourly air temperature ($^{\circ}\text{C}$), u_2 is the mean daily or hourly wind speed at a height of 2 m ($\text{m}\cdot\text{s}^{-1}$), e_s is the saturation vapour pressure (kPa), e_a is the actual vapour pressure (kPa), Δ is the slope vapour pressure curve ($\text{kPa } ^{\circ}\text{C}^{-1}$), γ is the psychrometric constant ($\text{kPa } ^{\circ}\text{C}^{-1}$), and C_n and C_d are coefficients that change depending on the calculation time step (hourly or daily) and reference vegetation type (ET_o for grass or ET_r for alfalfa).

2.4.3. Dual-Crop Coefficient Approach

The dual-crop coefficient approach is based on the standard method for estimating the crop ET (ET_c), which is calculated from ET_o and the crop coefficient (K_c). The FAO-56 dual-crop coefficient approach is based on crop transpiration and soil evaporation components [6,23]. The basal crop coefficient (K_{cb}) and soil evaporation coefficient (K_e) are considered in the dual-crop coefficient approach. In this study, ET_c values for paddy rice and longan in the testing area were determined using SIMDualKc software. SIMDualKc is a soil water balance model that estimates ET_c using the dual-crop coefficient approach [15,24]. Consequently, the ET_c value was calculated as follows:

$$ET_c = (K_s * K_{cb} + K_e) \times ET_o, \quad (10)$$

where K_{cb} is the basal coefficient, K_e is the soil evaporation coefficient, and K_s is the water stress coefficient. K_s ranges from 0 and 1 depending on the soil water content in the root zone. The K_{cb} of rice varies between 0.15 and 1.15, as suggested by Allen et al. [6] and Pereira et al. [23], and the K_{cb} of fruit trees varies between 0.75–1.15, as suggested by Allen et al. [6]. Date of each growing stage was obtained from the crop phenology identified by the NDVI. For the computation of K_e , soil data and soil evaporable layer data are required to compute the soil water balance in the root zone and the surface soil layer. As suggested

by Allen et al. [6], the SIMDualKc model provides values for the total available soil water, soil water content at field capacity, wilting point, and bulk density based on soil texture to assist users in selecting appropriate values for these parameters.

2.4.4. Estimation of Actual Evapotranspiration Based on the METRIC Model

Calculation of the Reference ET

In this step, weather data from the AWS at the Lamphun station were quality-assessed and quality-controlled before being used for the ET calculation. The weather data were then used as input for the REF-ET software to obtain the ET_{ref} equation at the time of satellite image acquisition, with hourly (for ET_r) and daily (for ET_r and ET_o) time steps.

METRIC Model Processing

The METRIC model was applied to estimate the ET_a from Landsat-8 images taken between October 2017 and May 2020, which covers the growth period in the dry season. Cloud masking was the first process applied to the satellite images in each scene. Hot pixels, representing empty agricultural fields without vegetation cover, and cold pixels, representing areas with full vegetation canopy, were selected for the study area. METRIC corresponds to the satellite-based surface energy balance. Thus, the latent heat flux (LE) was computed by subtracting the soil heat flux (G) and sensible heat flux (H) from the net radiation (R_n). The LE was computed for each pixel at the instant the satellite overpassed the monitored location and converted to ET_{inst} [9]. The ET_rF was then calculated as the ratio of ET_{inst} to ET_r at the time the satellite overpassed the monitored location and assumed to be equivalent to the 24 h average. Finally, ET_{24} was calculated by multiplying ET_rF by ET_r using the ET_{ref} equation.

Filling Image Gaps and Interpolation of the Daily Image

ET_rF and NDVI were used to fill data gaps due to cloud cover, provide missing values, and generate the daily ET_rF image between two dates of satellite image captures using the cubic spline interpolation method. Time series of daily ET_rF images was used to calculate the daily ET_a , and the NDVI was applied to extract crop phenology data and identify crop development stages, including initial, developing, middle, and late stages.

Spatiotemporal Distribution of ET_a for Various Land Use Types

Spatiotemporal distributions of ET_a for various land-use types were generated by multiplying the daily image of ET_rF by ET_r for each day. The output was ET_a , which was then accumulated over the period from October to May, covering the dry seasons in 2018, 2019, and 2020.

2.4.5. Evaluation of the Actual Evapotranspiration

In this study, the Muang Luang Irrigation Project was used as the field site for the testing area. Within this testing area, soil samples were collected, and soil properties were used as inputs for the SIMDualKc software, in addition to climate, crop, and irrigation data. For the crop data, each crop's planting date and crop growth period were required. This information was obtained from the crop phenology identified by the NDVI. The ET_a values obtained from METRIC and SIMDualKc were used for the evaluation. Finally, the accuracy of the ET_a values obtained from the METRIC and FAO-56 dual-crop coefficient methods was assessed using statistical analysis methods and the following quality measures: coefficient of determination (R^2), Root-Mean-Square Error (RMSE), and Mean Absolute Error (MAE).

3. Results and Discussion

3.1. Evaluation of the Actual Evapotranspiration

3.1.1. Analysis of the Crop Growth Period in the Testing Area during the Dry Season

Analysis of Landsat-8 satellite imagery collected between 1 November 2018 and 31 May 2019 showed that areas in which rice was cultivated accounted for 0.53 km² of the

testing area during this period. The rice-planting periods in each area differed due to the joint allocation of water. Farmers generally started planting rice in the southern part of the study area, followed by the northern part, with the period from the beginning of rice cultivation to harvest being ~120 days in length. The amplitudes of the NDVI values of each sampling plot were analysed during the growth period in the testing area. Typically, the peak NDVI occurs in the middle of the rice season. Thus, the start date of rice planting can be specified by counting back ~90 days from the date with the highest NDVI value, as shown in the NDVI graph of each area (Figure 3). In addition, the NDVI curve corresponds to K_{cb} , which was used at each stage of plant growth; this indicated that K_{cb} was the lowest in the initial stage, increased in the development stage, and peaked in the mid-season stage. The NDVI did not vary significantly for areas covered with longan as a perennial tree, with values ranging from ~0.4–0.6. Supriyasilp et al. [19] interviewed longan farmers and reported that the flowering period in this area ranges from February to May (dry season).

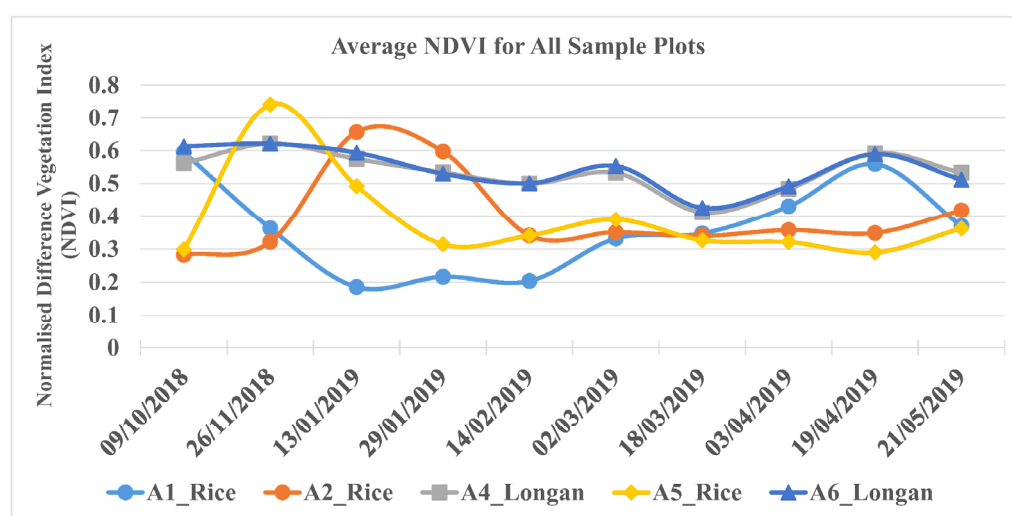


Figure 3. Crop phenology for plots in the testing area located in the Chom Thong District, Chiang Mai Province, downstream of the Muang Luang Weir in Thailand based on the Normalised Difference Vegetation Index (NDVI) in the dry season.

The farmers working on the land in the testing area first started cultivating rice in the A5_Rice sample plot, followed by the plots A2_Rice and A1_Rice (Figure 3). The highest NDVI values for these plots were observed on 26 November 2018, 13 January 2019, and 19 April 2019, respectively. Using these data, we identified the crops' planting dates and the crop growth periods of each sample plot. The K_{cb} and specific date of each plant growth stage were used as inputs for the crop section of the SIMDualKc. For the K_{cb} of rice, the values recommended by Allen et al. [6] and Pereira et al. [23] were used. A recommended value for the K_{cb} of longan was not available. Therefore, the K_{cb} value of fruit trees recommended by Allen et al. [6] was used. The SIMDualKc model was then utilised to estimate an ET_a value for comparison with the ET_a output of the METRIC model based on Landsat-8 satellite data.

3.1.2. Comparison of Actual Evapotranspiration Obtained from the METRIC Model and FAO-56 Method

The spatial distribution of the daily ET_a was obtained from the METRIC model based on Landsat-8 images with a resolution of 30 m in the testing area covering the dry season (1 October 2018 to 31 May 2019; Figure 4). The daily ET_a exhibited a significant spatial distribution and temporal changes across various land-use types and sample plots. The spatial distribution and temporal changes in ET_a during the dry season showed that the ET_a started to increase in February and reached its peak in April, corresponding to the crop growth period in irrigated agricultural areas. The spatial distribution and temporal

changes in the ET_r , showed the same patterns as those of the ET_a . Figure 4 shows the ET_a estimate obtained with METRIC, indicating that the ET_a was highest on 19 April 2019. Further, an average $ET_a > 7$ mm/day was observed in the A1 and A2 areas when rice was in its mid-season stage, and in the A4 and A6 areas, which contain longan orchards.

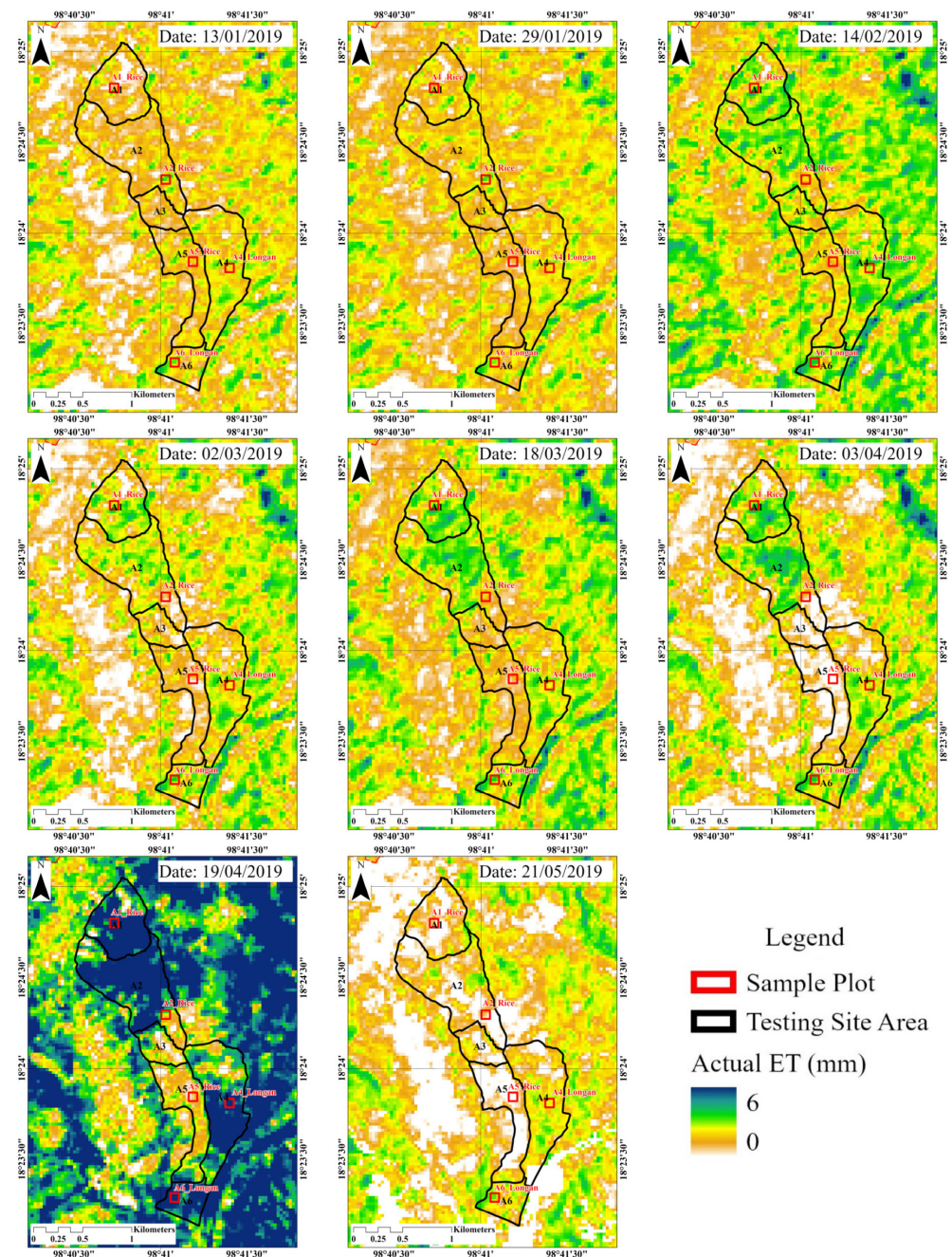


Figure 4. Daily actual evapotranspiration (ET_a) estimates for the testing area in the Chom Thong District, Chiang Mai Province, downstream of the Muang Luang Weir, Thailand, based on the mapping evapotranspiration at high resolution with internalized calibration (METRIC) model.

The spatiotemporal distribution obtained for the testing area is consistent with that reported by Supriyasilp et al. [19]: longan is mainly planted in A4 and A6. The amount of water required by longan trees is very high during March and April, i.e., the middle of the longan season. Farmers near the Ping River pump water from the river and directly supply it to the longan area.

Five sample plots in the testing area, including rice and longan plots, were used to evaluate the ET_a values obtained with the METRIC model relative to those obtained with the FAO-56 dual-crop coefficient method. Correlations between the daily ET_a from METRIC and SIMDualKc for each crop and all sample plots at the satellite acquisition date were evaluated (Figure 5). During the dry season in 2019, 34 observations ($N = 34$) were used to analyse the correlation between the ET_a from the METRIC model and that obtained from the SIMDualKc model (Figure 5). The data plots of the linear regression indicate that the ET_a estimates obtained from the METRIC model were strongly correlated with those obtained from SIMDualKc. The ET_a values based on METRIC and SIMDualKc were in good agreement. For the rice sample plots, the R^2 , RMSE, and MAE values were 0.827, 0.827, and 0.711 mm d⁻¹, respectively. For the longan sample plots, the R^2 , RMSE, and MAE values were 0.847, 0.631, and 0.455 mm d⁻¹, respectively. A comparison of the R^2 , RMSE, and MAE values between the rice and longan plots showed that the accuracy obtained for the longan plots was higher than that of the rice plots. The overall R^2 , RMSE, and MAE values of all sample plots (including rice and longan) were 0.830, 0.730, and 0.575 mm d⁻¹, respectively.

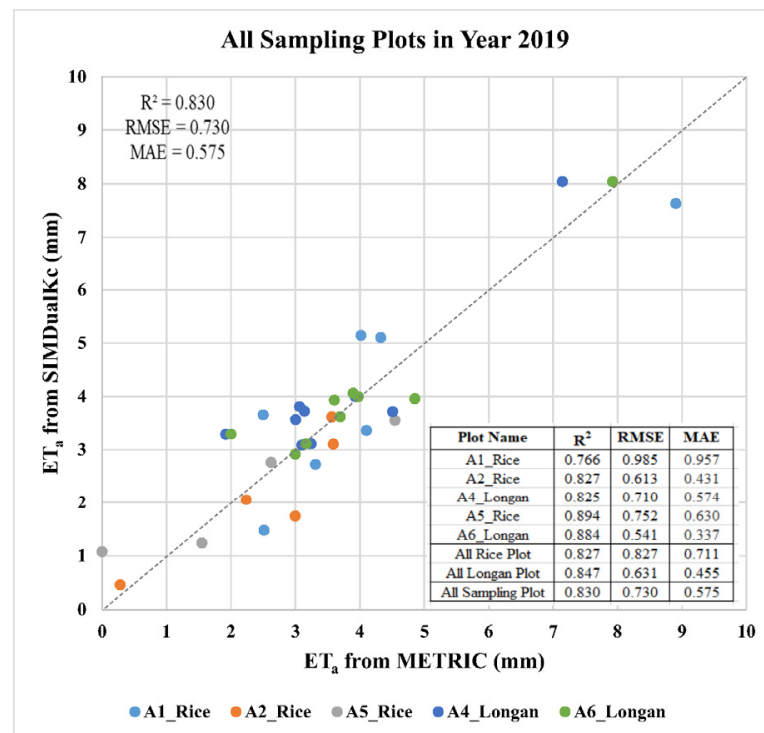


Figure 5. Correlation between the actual evapotranspiration (ET_a) values derived from the mapping evapotranspiration at high resolution with internalized calibration (METRIC) model and SIMDualKc at the satellite acquisition date for all sample plots from the testing area in the Chom Thong District, Chiang Mai Province, downstream of the Muang Luang Weir, Thailand.

The cumulative ET_a values derived from METRIC and SIMDualKc for each sample plot covering the dry season in 2019 were used to assess the accuracy of the seasonal ET_a (Table 5). Generally, rice was ready to be harvested 120 days after planting. Furthermore, the planting dates of the rice plots in the A2_Rice and A5_Rice plots did not significantly differ (Table 5). Both rice plots were planted in October and harvested from late January to mid-February. The A1_Rice plot was planted later than the other two plots. It was planted in mid-January and harvested in mid-May, with peak growth in April. We also found that ET_r was generally higher during March and May than in other months. Therefore, the cumulative ET_a of the rice plot in A1_Rice in the dry season was higher than that of the rice plots in A2_Rice and A5_Rice.

Table 5. Cumulative actual evapotranspiration (ET_a) values derived from the mapping evapotranspiration at high resolution with internalized calibration (METRIC) model and SIMDualKc for each sample plot in the testing area in the Chom Thong District, Chiang Mai Province, downstream of the Muang Luang Weir in Thailand, covering the dry season in 2019.

Plot Name	Seasonal Duration	Cumulative ET_a (SIMDualKc)	Cumulative ET_a (METRIC)	Percentage Difference (%)
A1_Rice	11/01/2019 to 11/05/2019	549.96	530.68	3.57
A2_Rice	17/10/2018 to 14/02/2019	328.14	318.85	2.87
A5_Rice	02/10/2018 to 29/01/2019	313.68	310.78	0.93
A4_Longan	01/11/2018 to 31/05/2019	817.99	755.14	7.99
A6_Longan	01/11/2018 to 31/05/2019	872.40	845.93	3.08
	Sum	2882.17	2761.38	4.28

The difference between the cumulative ET_a derived from SIMDualKc and that from the METRIC model ranged in magnitude from 0.93–3.57% for the rice and 3.08–7.99% for the longan sample plots. In all plots, the cumulative ET_a derived from METRIC was lower (4.28%) than that from SIMDualKc.

Tasumi [16] estimated the ET of the western Urmia Lake Basin using METRIC with Landsat satellite images from 2014–2016 for irrigated apple orchards, grape fields, and non-irrigated bare soil. The ET estimates obtained from METRIC (ET_{METRIC}) and the FAO-56 single-crop coefficient method (ET_{FAO56}) at the satellite image acquisition dates for the irrigated agricultural plots were in good agreement. The ET_{FAO56} and ET_{METRIC} differences for apple-planted, grape-planted, and bare soils were indicated by the RMSE, MAE, and Mean Bias Error (MBE), with values of 0.73, 0.84, and 0.68 mm d⁻¹ (positive numbers represent an overestimation); 0.57, 0.72, and 0.59 mm d⁻¹; and 0.20, 0.16, and 0.36 mm d⁻¹, respectively. Overall, the ET estimate from ET_{METRIC} was greater than that related to ET_{FAO56} . The error range indicated that wet apple fields had a high relative accuracy, while dry bare soil surfaces had a low relative accuracy. Similarly, Paço et al. [15] compared the ET at the dates of image acquisition derived from the METRIC model (ET_{METRIC}) and FAO-56 dual-crop coefficient method with that based on the SIMDualKc model (ET_{sim}). They reported that ET_{METRIC} and ET_{sim} had similar patterns. The overall MBE, defined as $(ET_{METRIC} - ET_{sim})/ET_{sim}$, between the ET derived from METRIC and that from SIMDualKc was 18% (the ET from METRIC was greater than the ET from SIMDualKc), corresponding to a mean absolute difference of 0.4 mm/d. Our results agree with previous reports [15,16], apart from the fact that the ET derived from METRIC was smaller than the ET derived from SIMDualKc. It is possible that ET_a was underestimated due to a lack of vegetation cover during the initial stage of crop growth [25,26], especially in the rice plots used in this study. In addition, METRIC uses a constant ET_r/F to estimate the daily ET_a ; as a result, water stress conditions may be underestimated. [7]. Furthermore, an underestimation of ET_a might have occurred due to an underestimation of the daily average R_n computed by empirical equations when upscaling the instantaneous ET_a to daily ET_a [26]. In addition, satellite pixels over small, cultivated fields may cause vegetation types and densities to mix, resulting in mixed surface temperature signals [7]. Therefore, it is difficult to interpret ET retrievals.

3.2. Spatiotemporal Distribution of the Actual Evapotranspiration for Various Land Use Types

3.2.1. Temporal Variation of the Actual Evapotranspiration

The ET variation and trends in northern Thailand are affected by rainfall and weather conditions. The average rainfall and humidity are lower during the dry season. Each year, the air temperature decreases to its minimum in December and increases to its maximum in April. The average ET_r from the AWS in the study area depends on the weather conditions. The average daily ET_a was obtained from the METRIC model for nine land-use types between October and May during the dry seasons in 2018–2020 (Figure 6). The average ET_r

decreased from October–December, with a minimum of 2.88 mm. It gradually increased in January, started to rapidly rise in February, and reached its peak in April (6.37 mm). The ET_a variation—mainly influenced by ET_r —for waterbodies was relatively consistent with the average trend in ET_r . The ET_a variation in forestland between October and February was consistent with the trend of ET_r , with the lowest ET_a in December (4.10 mm), when ET_a was greater than ET_r . From March–May, the ET_a/ET_r ratio decreased, and ET_a was lower than ET_r . The ET_a of miscellaneous land (mainly pastures in the study area) was related to the ET_a of natural vegetation, such as forests, but was smaller than that of forests. Perennial trees naturally grow without water management during the dry season and had slightly different monthly ET_a variations ranging from 2.55–3.26 mm. Field crops were primarily cultivated in non-irrigated areas. Field crops were planted during the rainy season and harvested between November and December. Their ET_a variations ranged from 3.07–3.68 mm, with slightly differing monthly ET_a values. Paddy fields in the study area were planted and harvested differently depending on the type of water management in the irrigated area. The ET_a for paddy fields was relatively consistent with the average trend in ET_r but lower than ET_r . The lowest and highest ET_a values were observed in December (1.67 mm) and April (2.78 mm), respectively. The ET_a variation of horticulture between October and January was consistent with the trend in ET_r . From February–May, the ratio of the ET_a to the ET_r of horticulture decreased, with the ET_a being lower than the ET_r . Orchards showed an ET_a pattern similar to that of perennial trees, with slightly different monthly ET_a variations. The lowest and highest ET_a estimates were obtained in November (2.6 mm) and May (3.13 mm), respectively. Finally, urban and built-up land showed the lowest ET_a values, with slightly different monthly ET_a variations. The average accumulated seasonal ET_a values for forestland, waterbodies, miscellaneous land, horticulture, field crops, perennial trees, orchards, paddy fields, and urban and built-up land over the dry seasons of 2018–2020 were 1,145.15, 1,067.65, 945.48, 935.97, 807.45, 664.76, 655.79, 547.29, and 511.27 mm, respectively (Table 6).

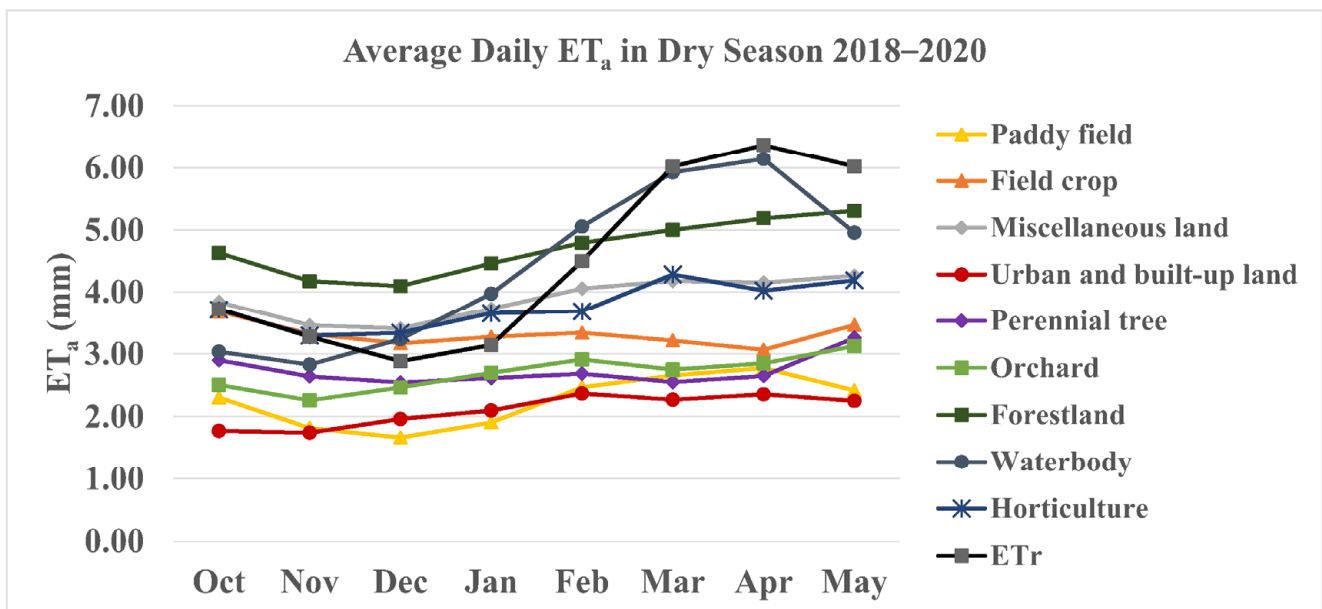


Figure 6. Average daily actual evapotranspiration (ET_a) and standardised alfalfa reference ET equation (ET_r) for nine land-use types in the study area in the Chiang Mai and Lamphun provinces, which are located on the plains of the upper northern region of Thailand along the Ping River, during the dry seasons of 2018–2020.

Table 6. Accumulated monthly and seasonal ET_a values for various land-use types and ET_r in the study area during the dry seasons of 2018, 2019, and 2020.

Date	ET_a (mm)									ET_r (mm)
	Paddy Field	Field Crop	Miscellaneous Land	Urban and Built-Up Land	Perennial Tree	Orchard Horticulture	Forestland	Waterbody		
2017/10/01 to 2017/10/31	82.16	100.69	110.94	59.45	88.68	80.01	107.76	132.36	90.09	110.09
2017/11/01 to 2017/11/30	58.76	82.01	94.47	50.56	67.52	62.10	95.66	113.74	66.14	93.51
2017/12/01 to 2017/12/31	55.06	85.99	98.18	62.87	76.20	74.17	97.97	117.83	86.48	87.71
2018/01/01 to 2018/01/31	57.93	94.99	114.70	65.35	86.50	84.99	111.73	141.24	120.49	94.61
2018/02/01 to 2018/02/28	60.37	81.20	105.68	58.78	75.21	75.29	104.76	130.49	125.54	115.45
2018/03/01 to 2018/03/31	58.15	66.96	102.36	44.70	59.66	59.46	103.86	128.14	134.18	170.43
2018/04/01 to 2018/04/30	55.86	65.24	101.39	43.65	64.16	61.37	100.17	135.63	136.11	170.84
2018/05/01 to 2018/05/31	83.67	112.58	137.49	73.51	122.52	105.04	128.70	171.64	157.21	165.49
Sum	511.96	689.66	865.22	458.86	640.44	602.44	850.61	1071.07	916.24	1008.13
2018/10/01 to 2018/10/31	69.31	106.17	110.40	46.62	81.18	66.75	104.69	135.40	82.59	113.48
2018/11/01 to 2018/11/30	73.95	120.14	118.28	73.29	110.63	87.86	110.60	138.60	108.19	98.85
2018/12/01 to 2018/12/31	59.08	97.38	103.05	66.00	85.42	78.75	99.61	118.51	107.29	87.05
2019/01/01 to 2019/01/31	54.90	97.24	109.97	56.14	75.00	76.20	109.45	132.00	104.14	94.61
2019/02/01 to 2019/02/28	75.85	93.41	116.08	64.75	73.26	82.40	115.02	136.79	139.07	131.77
2019/03/01 to 2019/03/31	85.97	85.84	122.92	61.86	64.40	78.04	126.09	150.08	180.29	187.3
2019/04/01 to 2019/04/30	130.36	112.32	158.11	98.47	102.09	115.45	157.23	192.03	243.42	204.21
2019/05/01 to 2019/05/31	62.72	77.75	112.59	54.62	73.67	74.14	115.71	142.46	135.50	195.71
Sum	612.12	790.25	951.39	521.76	665.64	659.61	938.39	1145.86	1100.51	1112.98
2019/10/01 to 2019/10/31	62.87	135.57	135.65	58.85	99.81	86.35	132.89	162.87	109.69	122.6
2019/11/01 to 2019/11/30	30.89	96.78	98.67	33.02	59.62	53.43	100.11	123.53	80.28	102.56
2019/12/01 to 2019/12/31	40.72	111.45	115.91	53.59	75.11	76.43	113.05	144.65	107.28	93.48
2020/01/01 to 2020/01/31	64.52	112.37	122.14	73.67	81.74	89.80	118.96	141.63	144.87	103.02
2020/02/01 to 2020/02/29	73.67	109.83	123.24	78.23	79.84	90.00	123.06	140.18	165.74	135.31
2020/03/01 to 2020/03/31	102.99	146.18	163.38	104.62	113.16	118.19	168.52	186.89	236.65	202.05
2020/04/01 to 2020/04/30	63.60	98.44	114.31	69.98	72.10	79.62	116.91	139.14	173.38	198.4
2020/05/01 to 2020/05/31	78.55	131.83	146.53	81.23	106.80	111.51	145.43	179.62	168.32	198.77
Sum	517.80	942.44	1,019.84	553.19	688.18	705.33	1018.92	1218.52	1186.20	1156.19
Average seasonal of ET_a (2018–2020)	547.29	807.45	945.48	511.27	664.76	655.79	935.97	1145.15	1067.65	1092.43

Our results show that the average daily ET_a of waterbodies was similar to the ET_r . Additionally, the ET_a values of forestland and waterbodies were higher than those of irrigated and non-irrigated agricultural areas, including rice, longan, and other land-use types, while the ET_a of urban areas was the lowest. These results are consistent with a previous report [27] which showed that forests and wetlands have higher average ET_a values than other land-use types, and that developed areas have the lowest average ET_a . Thus, ET_a appears to be determined by land use type, land cover, and water availability.

The spatiotemporal variation in ET_a depended on several factors controlling the ET rate, including weather, vegetation, soil, waterbodies, and management [17]. The ET trends of each land-use type were associated with their biophysical properties and factors controlling the ET. For example, forest areas are resistant to water stress in the regular dry season because the water storage in the soil's top 3 m layer is adequate for maintaining a stable ET rate [28]. Furthermore, the peak rate of ET was influenced by the height of vegetation. Forests have greater stomatal control than agricultural plants, which leads to higher ET values than other land-use types [17]. Similarly, urban and built-up land represent developed areas with lower ET_a values due to lower soil moisture availability [27].

3.2.2. Spatial Distribution of the Actual Evapotranspiration

The spatial distribution of the seasonal ET_a was calculated from accumulated time series of daily ET_a in the study area during the dry seasons of 2018, 2019, and 2020 (Figure 7). The characteristics of the ET_a distribution were consistent with variations in the climate, vegetation, and anthropogenic activities such as water resource management in the study area. The spatial distribution and variation of ET can be used as indicators of vegetation variation and water consumption [29]. Additionally, ET_a estimated from the METRIC model can capture crop water stress conditions [16].

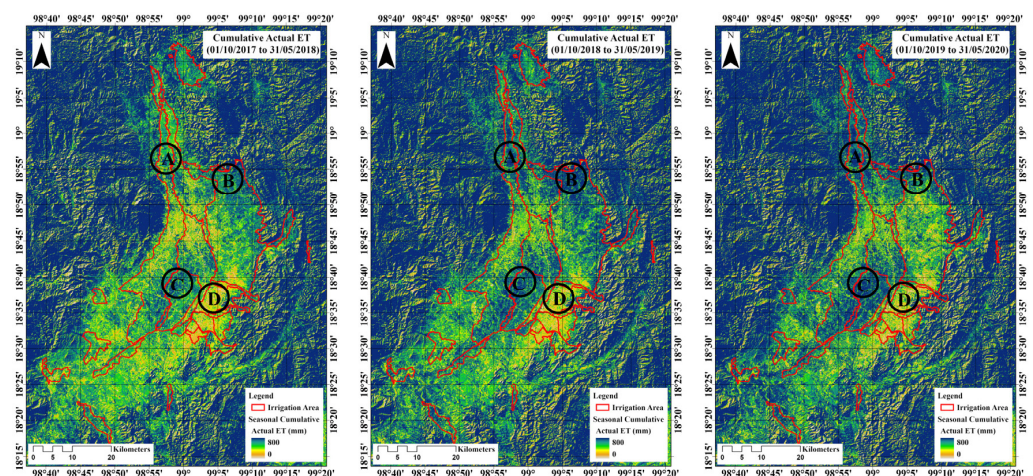


Figure 7. Spatial distribution of the seasonal actual evapotranspiration (ET_a) in the study area located in the Chiang Mai and Lamphun provinces, which is located on the plains of the upper northern region of Thailand along the Ping River, during the dry seasons of 2018–2020.

Within the study area, area A is an irrigated region belonging to two irrigation projects: Mae Tang and Mae Faek-Mae Ngat Somboon Chon (Figure 7). Area A is mainly covered by paddy fields; the ET_a in the cultivated area in the dry season is shown as the blue-shaded area in Figure 7. Areas B and D belong to the Mae Kuang Udom Thara irrigation project and are examples of upstream and downstream areas within the same irrigation project. Most rice-cultivation areas with adequate water allocation are located upstream of the irrigation project area (area B) and are shaded blue for all three years. Area D consists of primarily urban and built-up land in Lamphun Province. The paddy fields in area D were not cultivated during the dry season (shown as orange-shaded areas). In area C, which contains longan orchards, blue shading can be observed throughout the whole area

across all three years. As mentioned before, longan is an economically valuable fruit; thus, sufficient water is required for its maintenance.

4. Conclusions

In this study, satellite-based surface energy balance data derived from Landsat-8 imagery and the METRIC model were applied to estimate the spatiotemporal distribution of ET_a at a field scale, and to compare the ET_a obtained from the METRIC model with that derived from the FAO-56 dual-crop coefficient method using SIMDualKc.

The daily ET_a exhibited substantial spatial variation and temporal changes across various land-use types and sample plots in the testing area throughout the dry season. The accuracy of the ET_a values obtained from the METRIC model and FAO-56 dual-crop coefficient method was determined based on statistical analyses performed on the satellite acquisition dates and the cumulative ET_a of all sample plots. The data plots indicated that the ET_a estimates derived from the METRIC model were similar to those derived from SIMDualKc, and we observed a strong linear correlation between the estimates calculated using the two methods. Overall, the accuracy assessment for all sample plots on the satellite acquisition date yielded R^2 , RMSE, and MAE values of 0.830, 0.730, and 0.575 mm d⁻¹, respectively, and the ET_a accuracy obtained for the longan plots was higher than that for the rice plots. The differences between the cumulative ET_a derived from SIMDualKc and that derived from the METRIC model ranged in magnitude from 0.93%–3.57% and 3.08%–7.99% for the rice and longan sample plots, respectively. For all plots, the cumulative ET_a derived from METRIC was lower than that derived from SIMDualKc. Analysis of the ET_a variation for various land-use types showed that the average daily ET_a for waterbodies is similar to the ET_r . The ET_a values obtained for forestland and waterbodies were higher than those for irrigated and non-irrigated agricultural areas, including rice, longan, and other land-use types, while the ET_a for urban areas was the lowest. Overall, the observed spatial distributions and temporal changes of the seasonal ET_a during the dry seasons of 2018, 2019, and 2020 correlated with variations in the climate, vegetation, and anthropogenic activities such as water management in the study area each year.

The results of this study indicate that the METRIC model is an efficient tool for estimating ET_a during crop growth in the dry season, as well as the spatiotemporal distribution of the ET_a for various land-use types at a field scale, in order to facilitate water resource management. Furthermore, the METRIC model can be applied to estimate the spatiotemporal distribution of ET_a at field to regional scales, making it suitable for application to water resource management under various environmental conditions and for the improvement of the water use efficiency over a large area. In the future, ET_a studies should be expanded to other areas in Southeast Asia, as this region is an essential source of agricultural production.

Author Contributions: Conceptualisation, T.S. (Teerawat Suwanlertcharoen), T.S. (Thanaporn Supriyasilp) and K.P.; Formal analysis, T.S. (Teerawat Suwanlertcharoen); Investigation, T.S. (Teerawat Suwanlertcharoen); Methodology, T.S. (Teerawat Suwanlertcharoen); Supervision, T.C., T.S. (Thanaporn Supriyasilp) and K.P.; Visualisation, T.S. (Teerawat Suwanlertcharoen); Writing—original draft, T.S. (Teerawat Suwanlertcharoen); Writing—review and editing, T.S. (Thanaporn Supriyasilp). All authors have read and agreed to the published version of the manuscript.

Funding: This research received no external funding.

Data Availability Statement: Data will be provided upon request.

Acknowledgments: We thank the Thai Meteorological Department for providing the climate and rainfall data used in this study. We also thank the Land Development Department for providing the land-use data used in this study.

Conflicts of Interest: The authors declare no conflict of interest.

References

1. Takeshima, H.; Joshi, P.K. *Overview of the Agricultural Modernization in Southeast Asia*; IFPRI Discussion Paper 1819; International Food Policy Research Institute (IFPRI): Washington, DC, USA, 2019. [CrossRef]
2. Association of Southeast Asian Nations. ASEAN Statistical Yearbook 2020. 2021. Available online: https://aseandse.org/wp-content/uploads/2021/02/ASYB_2020.pdf (accessed on 30 October 2021).
3. Altendorf, S. Minor Tropical Fruits (Mainstreaming a Niche Market). *Food Outlook* **2018**, *8*, 67–75. Available online: http://www.fao.org/fileadmin/templates/est/COMM_MARKETS_MONITORING/Tropical_Fruits/Documents/Minor_Tropical_Fruits_FoodOutlook_1_2018.pdf (accessed on 21 March 2022).
4. Mancosu, N.; Snyder, R.L.; Kyriakakis, G.; Spano, D. Water scarcity and future challenges for food production. *Water* **2015**, *7*, 975–992. [CrossRef]
5. Spreer, W.; Schulze, K.; Ongprasert, S.; Wiriya-Alongkorn, W.; Müller, J. Mango and longan production in northern Thailand: The role of water saving irrigation and water stress monitoring. In *Sustainable Land Use and Rural Development in Southeast Asia: Innovations and Policies for Mountainous Areas*; Fröhlich, H.L., Schreinemachers, P., Stahr, K., Clemens, G., Eds.; Springer Environmental Science and Engineering; Springer: Berlin, Germany, 2013; pp. 215–228. [CrossRef]
6. Allen, R.G.; Pereira, L.S.; Raes, D.; Smith, M. *Crop evapotranspiration-Guidelines for computing crop water requirements-FAO Irrigation and drainage paper 56*; FAO: Rome, Italy, 1998; Volume 300, p. D05109.
7. Allen, R.G.; Pereira, L.S.; Howell, T.A.; Jensen, M.E. Evapotranspiration information reporting: I. Factors governing measurement accuracy. *Agric. Water Manag* **2011**, *98*, 899–920. [CrossRef]
8. Bastiaanssen, W.G.M.; Menenti, M.; Feddes, R.A.; Holtslag, A.A.M. A remote sensing Surface Energy Balance Algorithm for Land (SEBAL). *J. Hydrol.* **1998**, *212–213*, 198–212. [CrossRef]
9. Allen, R.G.; Tasumi, M.; Trezza, R. Satellite-based energy balance for Mapping Evapotranspiration with Internalized Calibration (METRIC)—Model. *J. Irrig. Drain. Eng.* **2007**, *133*, 380–394. [CrossRef]
10. Allen, R.G.; Irmak, A.; Trezza, R.; Hendrickx, J.M.H.; Bastiaanssen, W.; Kjaersgaard, J. Satellite-based ET estimation in agriculture using SEBAL and METRIC. *Hydrol. Process* **2011**, *25*, 4011–4027. [CrossRef]
11. Zheng, C.; Jia, L.; Hu, G.; Lu, J. Earth observations-based evapotranspiration in northeastern Thailand. *Remote Sens.* **2019**, *11*, 138. [CrossRef]
12. Sriwongsitanon, N.; Suwawong, T.; Thianpopirug, S.; Williams, J.; Jia, J.; Bastiaanssen, W. Validation of seven global remotely sensed ET products across Thailand using water balance measurements and land use classifications. *J. Hydrol. Reg. Stud.* **2020**, *30*, 100709. [CrossRef]
13. Kosa, P.; Pongput, K.; Nontananandh, S.; Khobklay, P. Spatial and temporal distribution of irrigation requirements in the Chao Phraya River Basin, Thailand. *Kasetsart J. Nat. Sci.* **2008**, *42*, 758–766.
14. Maskong, H.; Kosa, P.; Jothityangkoon, C. Estimation of evapotranspiration in Lam Ta Kong Basin using Surface Energy Balance Algorithm for Land (SEBAL) Model. In Proceedings of the THA 2015 International Conference on Climate Change and Water & Environment Management in Monsoon Asia, Bangkok, Thailand, 28–30 January 2015.
15. Paço, T.A.; Pôças, I.; Cunha, M.; Silvestre, J.C.; Santos, F.L.; Paredes, P.; Pereira, L.S. Evapotranspiration and crop coefficients for a super intensive olive orchard. An Application of SIMDualKc and METRIC models using ground and satellite observations. *J. Hydrol.* **2014**, *519*, 2067–2080. [CrossRef]
16. Tasumi, M. Estimating evapotranspiration using METRIC Model and Landsat data for better understandings of regional hydrology in the Western Urmia lake basin. *Agric. Water Manag* **2019**, *226*, 105805. [CrossRef]
17. Jensen, M.E.; Allen, R.G. *Evaporation, Evapotranspiration, and Irrigation Water Requirements*, 2nd ed.; American Society of Civil Engineers: Reston, VA, USA, 2016.
18. HAIL. Data Warehouse System Development Project of 25 Basin and Flood and Drought Modeling: Ping Basin. [in Thai]. 2012. Available online: <https://tiwrm.hii.or.th/web/attachments/25basins/06-ping.pdf> (accessed on 31 October 2021).
19. Supriyasilp, T.; Pongput, K.; Boonyanupong, S.; Suwanlertcharoen, T. Enhanced water management for Muang Fai irrigation systems through remote sensing and SWOT analysis. *Water Resour Manag.* **2021**, *35*, 263–277. [CrossRef]
20. Supriyasilp, T.; Pongput, K. Water Balance Model as a tool for building participation and joint water use promotion at the river basin level. *Irrig. Drain* **2021**, *70*, 254–268. [CrossRef]
21. Tasumi, M. Progress in Operational Estimation of Regional Evapotranspiration Using Satellite Imagery. PhD Dissertation, University of Idaho, Moscow, Russia, 2003.
22. Allen, R.G.; Burnett, B.; Kramber, W.; Huntington, J.; Kjaersgaard, J.; Kilic, A.; Kelly, C.; Trezza, R. Automated calibration of the METRIC-Landsat Evapotranspiration Process. *J. Am. Water Resour. Assoc.* **2013**, *49*, 563–576. [CrossRef]
23. Pereira, L.S.; Paredes, P.; López-Urrea, R.; Hunsaker, D.J.; Mota, M.; Mohammadi Shad, Z. Standard single and basal crop coefficients for vegetable crops, an Update of FAO56 Crop Water Requirements Approach. *Agric. Water Manag.* **2021**, *243*, 106196. [CrossRef]
24. Rosa, R.D.; Paredes, P.; Rodrigues, G.C.; Fernando, R.M.; Alves, I.; Pereira, L.S.; Allen, R.G. Implementing the dual crop coefficient approach in interactive software: 2. Model Testing. *Agricultural Water Manag.* **2012**, *103*, 62–77. [CrossRef]
25. Mkhwanazi, M.; Chávez, J.L.; Andales, A. SEBAL-a: A remote sensing ET algorithm that accounts for advection with limited data. Part I: Development and Validation. *Remote Sens.* **2015**, *7*, 15046–15067. [CrossRef]

26. Xue, J.; Bali, K.M.; Light, S.; Hessels, T.; Kisekka, I. 2020. Evaluation of remote sensing-based evapotranspiration models against surface renewal in almonds, tomatoes and maize. *Agric. Water Manag.* **2020**, *238*, 106228. [[CrossRef](#)]
27. Liu, W.; Hong, Y.; Khan, S.I.; Huang, M.; Vieux, M.; Caliskan, S.; Grout, T. Actual evapotranspiration estimation for different land use and land cover in urban regions using Landsat 5 data. *J. Appl. Remote Sens.* **2010**, *4*, 041873. [[CrossRef](#)]
28. Khand, K.; Numata, I.; Kjaersgaard, J.; Vourlitis, G.L. Dry season evapotranspiration dynamics over human-impacted landscapes in the Southern Amazon using the Landsat-based METRIC Model. *Remote Sens.* **2017**, *9*, 706. [[CrossRef](#)]
29. Liu, J.; Xiong, Y.; Tian, J.; Tan, Z. Spatiotemporal changes in evapotranspiration from an overexploited water resources basin in arid northern China and their implications for ecosystem management. *Sustainability* **2019**, *11*, 445. [[CrossRef](#)]

Disclaimer/Publisher's Note: The statements, opinions and data contained in all publications are solely those of the individual author(s) and contributor(s) and not of MDPI and/or the editor(s). MDPI and/or the editor(s) disclaim responsibility for any injury to people or property resulting from any ideas, methods, instructions or products referred to in the content.